Detecting Partial Demagnetization in AFPM Generators by Monitoring Speed and EMF Induced in a Supplemental Winding

Detecting Partial Demagnetization in AFPM Generators by Monitoring Speed and EMF Induced in a Supplemental Winding

***Abstract*—In this paper, a novel method to detect the partial demagnetization in air-cored permanent-magnet (PM) Axial-Flux generators is proposed. Its principle is to monitor a speed-normalized fault detection signal. This signal depends only on the demagnetization severity, as it was extracted using a flux-sensor with a span that negates the induced voltage under balanced conditions. The generator has been designed for marine renewable applications working under variable speed conditions rending PM health monitoring under nonstationary conditions imperative. Initially, a mathematical equation for the electromotive force (EMF) is derived under partial demagnetization conditions with the aim to extract the frequency components related to the fault. To estimate the demagnetization severity, an approach was developed based on the magnetic flux monitoring, which penetrates throughout the sensor. A 3-D finite-element model of the installed winding in the generator is employed to verify the proposed method under steady and variable speed conditions.**

***Index Terms*— Axial-Flux PM Generators, Partial demagnetization, fault diagnosis, Tidal current turbine.**

I. Introduction

AXIAL flux PM machines have been investigated to a significant degree during the past two decades, as they appear to be an attractive alternative to the conventional radial flux machines due to their higher torque density, compact construction and the feature to embed multiple stages together in a single construction [1]. High operational temperatures, armature reaction fields, oxidation, corrosion, manufacturing defects are the main reasons which rend all brushless PM machines to faulted operations [2]. More specifically, matullurgical variations in the material at high operating temperatures and oxidation lead a permanent-magnet in irreversible demagnetization. NdFeB magnets are prone to irreversible demagnetization due to poor thermal characteristics, low corrosion resistance under humid enviroments, and poor mechanical streingth which leads to decomposition due to corrosion, cracks or loss of small pieces in the edges [3]–[6]. The partially demagnetized machines demand a higher stator current to develop the same quantity of electromagnetic torque, causing serious thermal insulation stress, which significantly reduces their life expectancy [7]. Moreover, partial demagnetization increases the magnitude of higher force harmonic components leading tovibration and acoustic noise radiated from the machine [8] and
alters the attraction between the rotor and the stator leading to a change in the machines' shaft trajectory [9].
Generally there is a significant amount of work that has been done on the detection of the partial demagnetization fault in the past two decades [3], [5], [10]–[12].

Diagnostic methods based on the signature analysis of the machines' parameters on frequency domain have been developed for the detection of the partial demagnetization fault based on the frequency domain. These methods are capable not only of detecting this specific fault online, but also distinguishing it with the dynamic eccentricity, as the two faults induce frequency components with the mechanical speed on machine quantities [11], [13].

However, these techniques use as fault index signature components in which their amplitudes are severely influenced by the winding configuration, [14]. As a result, in PM machines with parallel path windings, the current amplitude frequency components in branches can be used as a fault indicator [15]. PM machines with parallel path windings generate circulating currents which flow between the branches depending on the impact of the fault on the field distribution [16], as it greatly influences these currents [17].

Flux-based fault detection techniques using commercial flux sensors [12], [18]–[20] or by using a number of search coils with a proper span [21]–[23] is a reliable, low-cost and industrial applied method to extract fault indicator quantities. Their major advantage is the ability to measure the flux at various points and for specific surfaces in an electric machine; as a result, making it possible to exploit the consequences of a fault. By mounting search coils in the teeth of a PMSM, all faults can be detected and distinguished as every polar plot is unique [23]. Static eccentricity creates two air-gap regions where the air-gap has a higher or lower length compared two the healthy state and also two points where the air-gap variation is negligible. The aforementioned means that three search coils are required in order to detect the severity and minimum air-gap position of this fault [21]. A search coil was used to detect dynamic eccentricity [22] by monitoring the peak-to-peak magnitude of the speed normalized-voltage in time because the signal is zero as it is spanned 3 coils - 4 pole pitches.

Partial demagnetization fault under transient operating conditions can be detected using time-frequency based signal processing algorithms in which every algorithm uses different transformation functions. STFT [24] has a steady window length, so fast transients cannot be analyzed with high resolution. CWT and DWT have a variable window length, so they are more appropriate for nonstationary signals with more rapid dynamics [5].

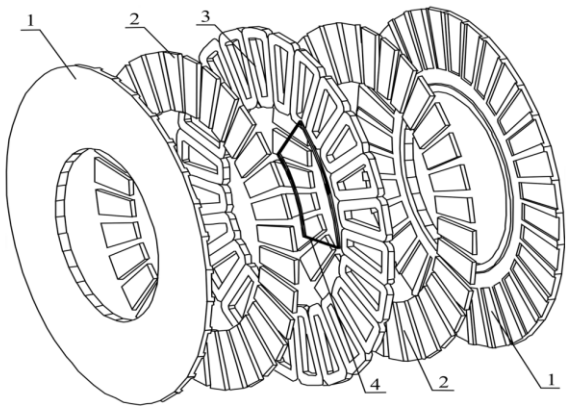

Fig. 1. Exploded wireframe model of the analyzed AFPM generator with the supplemental winding corresponding to a span of 3 coils and 4 pole pitches. (1) Rotor disc, (2) PM, (3) armature coil, and (4) supplemental winding.

This paper proposes a method to detect partial demagnetization in axial-flux permanent magnet machines with the use of a supplemental winding on the air-gap with a span that negates the voltage. On a speed-transient state, the voltage signal has been normalized by the mechanical speed. Finally, Fig. 1 illustrates the wireframe model in an exploded view of the AFPM generator carrying the supplemental winding.

II. Mathematical Derivation of EMF Due to Partial Demagnetization

A. EMF induced in a single coil of the stator winding under balanced conditions

When the rotor of a coreless AFPM generator exhibits concentric motion without any fault on it, the air-gap length of the machine is constant, no matter the position of the rotor. The air-gap length of an air-cored double-rotor-single-stator AFPM generator can be considered as constant since there is no stator slotting effect; there is only the saliency effect, but in this analysis it is neglected. The air-gap length under healthy conditions is:

$$g_{ideal} = 2h_{PM} + 2g + t_w \tag{1}$$

Where h_{PM}, g, and t_w are the magnet height, the mechanical magnet to coil clearance, and the stator winding thickness. The air-gap permeance for a coreless AFPM generator without partial demagnetization or any other kind of fault is constant, and it is given by the following equation:

$$\Lambda_{ideal} = \frac{\mu_0}{2\frac{h_{PM}}{\mu_{rrec}} + 2g + t_w} \tag{2}$$

where μ_o, and μ_{rrec} is the permeability of free space and the relative recoil permeability of the magnet ($\mu_{rrec} \approx 1$). For Nd-Fe-B magnets under low operational temperature, their BH characteristic can be considered approximately linear. The magneto-motive force (MMF) *F* developed from the PMs can be expressed using Fourier series composition as follows:

$$F(\theta,t) = \sum_{\nu=2\mu+1}^{\infty} F_{PM,\nu} \cos(\nu p\theta - \nu\omega_s t - \varphi_\nu) \tag{3}$$

where μ=0,1,2,…, $F_{PM,\nu}$, φ_ν, p, θ, ω_s, and t are the magnitude, phase angle of the MMF for the ν^{th} contextually harmonic component, the number of pole pairs, an angle from a reference axis, angular electrical speed and the time variable, the magnetic flux density can be written as a product of the relative air-gap permeance function the PM magneto-motive force:

$$B = \Lambda \cdot F \tag{4}$$

Expanding (2) with binomial series and neglecting higher-order terms and then substituting the final expansion and (3) to (4) and executing the algebraic calculations it yields:

$$B(\theta,t) = \alpha \sum_{\nu=2\mu+1}^{\infty} F_{PM,\nu} \cos\left(\nu p\theta - \nu\omega_s t - \varphi_\nu\right) \tag{5}$$

Where α is a constant depending on the generator's geometrical dimensions, given in the appendix. In order to calculate the magnetic flux Φ, the magnetic flux density wave along the middle air-gap facing an armature coil is integrated. Considering an angle element dθ which corresponds to a surface dS on the coil which a magnetic flux element dΦ penetrates through it. The magnetic flux can be formulated as follows:

$$\Phi_\xi(t) = \frac{(r_o - r_i)^2}{2} \int_{\frac{2\pi}{c}(\xi-1)}^{\frac{2\pi}{c}\xi} B(\theta,t)d\theta \tag{6}$$

where r_o, r_i, c, and ξ are the outer and inner radius of the PMs, the total number of stator winding coils, and the ξ^{th} coil. The EMF induced in the ξ^{th} coil winding $E_\xi(t)$ can be calculated as the time derivative of the magnetic flux penetrating through the ξ^{th} coil with respect to time as follows:

$$E_\xi(t) = -N_c \cdot \frac{d\Phi(t)}{dt} \tag{7}$$

where N_c is the number of turns in a coil. After substituting (5) into (6), integrating along the middle of one of two air-gaps, and then differentiating with respect to time, the EMF induced in the ξ^{th} armature coil winding of the AFPM generator, under healthy conditions, can be mathematically illustrated as follows:

$$E_\xi(t) = \frac{\alpha(r_o - r_i)^2 N_c \omega_r}{2} \cdot \sum_{\nu=2\mu+1}^{\infty} F_{PM,\nu} \left\{ \cos\left(\nu p \frac{2\pi}{c}(\xi-1) - \nu\omega_s t - \varphi_\nu \right) - \cos\left(\nu p \frac{2\pi}{c}\xi - \nu\cdot\omega_s t - \varphi_\nu \right) \right\} \tag{8}$$

where ω_r is the mechanical speed. For a PM generator under balanced conditions, the induced EMF in the ξ^{th} coil distributed symmetrically in space along the periphery of the stator contains higher harmonic components that distort the fundamental one. Equation (8) expresses that in the ξ^{th} stator coil will be induced harmonic components with frequencies νf_s. The voltage in the analysis mentioned above describes the EMF or no-load voltage because the magnetic field created by the armature winding has not been taken into consideration. The induced voltage on the supplemental winding can be found by integrating the flux over the surface of the winding which is 4 pole pitches, by substituting (5) into (6) and integrating over four pole pitches.

B. EMF Induced in the supplemental winding due to partial demagnetization

In order to calculate the EMF under partial demagnetization, the proper relative air-gap permeance function needs to be extracted. In this condition, the magnetic flux density wave has

a minor reduction on the specific pole pitch. This means that the air-gap is not constant, but we can consider that its length is increased in that particular magnet pitch—the magnet moves, which means that this increased air-gap length rotates with the mechanical rotational speed.

In Fig. 2, the air-gap length and the relative permeance is shown along a circle in the mid radius of the magnets under healthy and partial demagnetization conditions. When the magnet is demagnetized, the air-gap increases with the fault severity, and it can be represented as D=εg where ε>1 is a factor corresponding to the increment and D can be considered a factor which is related directly to the fault severity. Moreover, the air-gap permeance in the same angle-pitch will be reduced by ε′Λ since fewer magnetic lines will remain in that area. Utilizing the aforementioned logic, the air-gap under partial demagnetization is both a function of space and time:

$$g_{demag}(\theta,t)=2\frac{h_{PM}}{\mu_{rrec}}+2g+t_w+D\left\{\frac{1}{2p}+\sum_{k=1}^{\infty}\frac{2}{k\pi}\sin\left(\frac{k\pi}{2p}\right)\cos\left(k\theta-k\omega_r t\right)\right\} \quad (9)$$

where the last term of the above equation is a constructed pulse wave using Fourier series, which moves with the mechanical rotational speed ω_r, as the demagnetized magnet does.

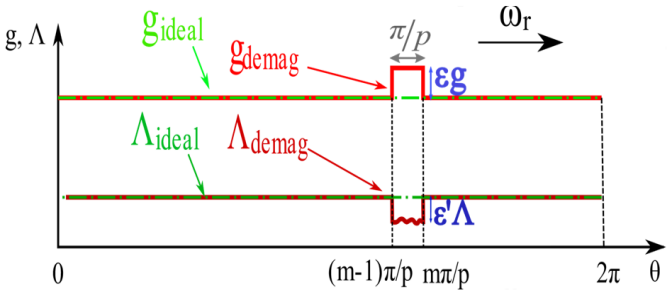

Fig. 2. The air-gap length along the periphery at a mid radius of the PMs and the air-gap permeance, under healthy and demagnetized conditions.

The relative permeance function under partial demagnetization can be represented as follows:

$$\Lambda_{demag}(\theta,t)=\frac{\mu_0}{2\frac{h_{PM}}{\mu_{rrec}}+2g+t_w+D\left\{\frac{1}{2p}+\sum_{k=1}^{\infty}\frac{2}{k\pi}\sin\left(\frac{k\pi}{2p}\right)\cos\left(k\theta-k\omega_r t\right)\right\}} \quad (10)$$

The above-equation may be further written in the form below:

$$\Lambda_{demag}(\theta,t)=\frac{\mu_0}{2h_{PM}}\left\{\begin{aligned}&1+\frac{g}{h_{PM}}+\frac{t_w}{2h_{PM}}\\&+\left\{\frac{D}{4h_{PM}p}+\sum_{k=1}^{\infty}\frac{D}{k\pi h_{PM}}\sin\left(\frac{k\pi}{2p}\right)\cos\left(k\theta-k\omega_r t\right)\right\}\end{aligned}\right\}^{-1} \quad (11)$$

The above equation has been formulated in such a manner to be expanded using the binomial Taylor series. After its expansion, the eventual relative permeance function having one pole pitch demagnetized is:

$$\Lambda_{demag}(\theta,t)=a+\beta(D)+\gamma(D)\cdot\sum_{k=1}^{\infty}\cos\left(k\theta-k\omega_r t\right) \quad (12)$$

where β, and γ are two constants depending on the generator parameters and partial demagnetization factor, and are given in the appendix. It should be noted that β(0)=γ(0)=0. The MMF can be represented using Fourier series similarly using equation (3) with the only difference that the amplitude of every component will be different due to the demagnetization. After employing (4) again, and taking into consideration equation which connects the rotational speed with the electrical speed (13), the air-gap magnetic flux density wave with the fault embedded can be calculated as follows:

$$\omega_r=\frac{\omega_s}{p} \quad (13)$$

$$B_{demag}(\theta,t)=\left(\alpha+\beta(D)\right)\cdot\sum_{\nu=2\mu+1}^{\infty}F_{PM,\nu}^{demag}\cos\left(\nu p\theta-\nu\omega_s t-\varphi_\nu\right)+$$
$$+\frac{\gamma(D)}{2}\sum_{\nu=2\mu+1}^{\infty}\sum_{k=1}^{\infty}F_{PM,\nu}^{demag}\left\{\begin{aligned}&\cos\left(\left(\nu p-k\right)\theta-\left(\nu-\frac{k}{p}\right)\nu\omega_s t\right)\\&+\cos\left(\left(\nu p+k\right)\theta-\left(\nu+\frac{k}{p}\right)\omega_s t\right)\end{aligned}\right\} \quad (14)$$

After substituting equation (14) into (6), integrating along the middle air-gap facing three coils or four-pole pitches the first term of (14) will be cancelled and afterwards differentiating with respect time using (7), yields:

$$E_{demag}(t)=\frac{1}{4}N_c\gamma(D)\left(r_o^2-r_i^2\right)\omega_r\sum_{\nu=2\mu+1}^{\infty}\sum_{k=1}^{\infty}F_{PM,\nu}^{demag}\left\{\begin{aligned}&\cos\left(\left(\nu p-k\right)\frac{4\pi}{p}-\left(\nu-\frac{k}{p}\right)\omega_s t\right)\\&-\cos\left(\left(\nu-\frac{k}{p}\right)\omega_s t\right)\\&+\cos\left(\left(\nu p+k\right)\frac{4\pi}{p}-\left(\nu+\frac{k}{p}\right)\omega_s t\right)\\&-\cos\left(\left(\nu+\frac{k}{p}\right)\omega_s t\right)\end{aligned}\right\} \quad (15)$$

The EMF induced in the supplemental winding will have additional time-harmonic components under a stationary rotational speed, which depends on the pole pair number of the AFPM generator. These additional harmonic components have amplitudes which are increasing with the degree D^2+D, according to the appendix, and their frequencies are:

$$f_{demag}=\left(\nu\pm\frac{k}{p}\right)\cdot f_s \quad (16)$$

where ν=2μ+1 is a positive odd number as μ=0,1,2,… and k=1,2,3,….The amplitudes with frequency patterns given by (16) of the voltage on the additional winding, normalized by the speed, can be used as a fault indicator as these amplitudes depend on only the fault severity, which gives the major advantage of monitoring for the specific fault under variable speed conditions.

C. EMF Induced in a phase winding due to partial demagnetization

For an AFPM generator with in-series coils of a phase, the EMF induced in an entire phase can be calculated by adding the instantaneous values for every coil separately distributed in space, the generalized equation is the following:

$$E_{demag,ph}(t)=\frac{1}{4}(\alpha+\beta(D))(r_o-r_i)^2 N_c\omega_r\sum_{\xi=1}^{N_{cs}}\sum_{\nu=2\mu+1}^{\infty}F_{PM,\nu}^{demag}\left\{\begin{matrix}\cos\left(\nu p\frac{2\pi}{c}(\xi-1)-\nu\omega_s t-\varphi_\nu\right)\\-\cos\left(\nu p\frac{2\pi}{c}\xi-\nu\omega_s t-\varphi_\nu\right)\end{matrix}\right\}+ \quad (17)$$

$$\frac{1}{4}\gamma(D)(r_o-r_i)^2 N_c\omega_r\sum_{\xi=1}^{N_{cs}}\sum_{\nu=2\mu+1}^{\infty}\sum_{k=1}^{\infty}F_{PM,\nu}^{demag}\left\{\begin{matrix}\cos\left((\nu p-k)\frac{2\pi}{c}\xi-\left(\nu-\frac{k}{p}\right)\omega_s t-\varphi_\nu\right)-\\\cos\left((\nu p-k)\frac{2\pi}{c}(\xi-1)-\left(\nu-\frac{k}{p}\right)\omega_s t-\varphi_\nu\right)\\+\cos\left((\nu p+k)\frac{2\pi}{c}(\xi-1)-\left(\nu+\frac{k}{p}\right)\omega_s t-\varphi_\nu\right)\\-\cos\left((\nu p+k)\frac{2\pi}{c}\xi-\left(\nu+\frac{k}{p}\right)\omega_s t-\varphi_\nu\right)\end{matrix}\right\}$$

where, ξ=1,2,.., $N_{cs,}$ and N_{cs} is the total number of coils which a phase contains. The specific generator has 4 parallel paths in an 8 coil phase winding, so according to the above equation, the partial sums for ξ=1 and ξ=2 should be used for the calculation as the other coil pairs will have equal voltages due to their electric parallel connection. All coils will have the harmonics of equation (17), but these harmonics are in various phases with each other due to the spatial distribution of coils along the generator's periphery. Afterwards, depending on the way that these coils connect with each other, the components related to the partial demagnetization fault may cancel with each other or affect their amplitudes depending on the winding configuration. This means that these amplitude components are influenced by the way that coils of a phase are connected, and a PM machine with different winding connections will have different outcomes on these fault signature components [16]. Therefore, (17) shows that alterations in partial demagnetization cannot be identified with high reliability by monitoring the EMF or the load voltage in a phase winding.

D. Analytical prediction of the demagnetization severity

In this subsection, the level of demagnetization is calculated theoretically using the geometry of the supplemental winding. According to [26], in an AFPM machine with two rotor discs, the main magnetic field lines that induce the armature voltage are between the opposite magnets in the discs. There are also field lines that flow between the adjacents magnets of each disc, and these also contribute to the voltage generation. Additionally, there is the PM rotor leakage field, which contains all the lines which do not penetrate through the stator coils and the stator leakage field, which does not contribute to the interaction with the main PM rotor field.

When all magnets are healthy, the vector sum of magnetic flux which penetrates through the search coil is zero, which means that there is no voltage induction. For every arbitrary angle of the rotating magnetic field, the total magnetic flux crossing through the additional winding will be zero too. When at least one magnet is demagnetized, the number of the magnetic flux lines in a single-pole pitch reduces, and as this magnet transits through the search coil, the vector sum of the magnetic flux ceases to be zero. As a result, an alternating voltage is generated on the terminals of the search coil. The currents in three coils are in a 120° phase difference, which means that the magnetic flux of each coil also has the same phase difference, hence the resultant magnetic flux, which crosses through the supplemental winding is zero due to the armature under healthy conditions.

Fig. 3 illustrates the 2-D view geometry of the additional winding, which occupies 4 pole pitches and 3 coil pitches along the generator periphery, for a specific rotor position. The magnetic field waveform, which corresponds to each magnet on that arbitrary position, is also presented. The last permanent magnet on the same figure is demagnetized, and this was modeled by the reduction of the magnetic field on that specific pitch.

The fundamental harmonic of the flux density wave at a time instant can be written as follows [27]:

$$B(\theta)=B_g\sin\left(p\theta\right) \quad (19)$$

where B_g is the magnetic field density amplitude of the wave in the middle o fthe air-gap point where the additional winding is located. This value depends on the magnet height, h_{PM}, air-gap thickness, which in this coreless AFPM generator is given by (1) and from the relative recoil permeability of the PM, μ_{rrec}.

$$\frac{B_r}{\mu_0\mu_r}2h_{PM}=\frac{2B_g}{\mu_0\mu_r}2h_{PM}+\frac{B_g}{\mu_0}2g+\frac{B_g}{\mu_0}2t_w \quad (20)$$

$$B_g=\frac{B_r}{1+\mu_r\frac{g+0.5t_w}{h_{PM}}} \quad (21)$$

According to Fig. 3, an angle element on the additional winding occupies a surface element dS, and through this surface, an element magnetic flux element penetrates from it. The surface element of one pole pitch is given as follows [27]:

$$dS=\frac{\pi}{p}r\cdot dr \quad (22)$$

By substituting into (6), (19) and integrating in the counterclockwise direction along the air-gap facing the additional winding when the magnetic flux density wave is in the position of Fig. 3, yields the following integral summation:

$$\Phi(\theta)=\left\{\begin{matrix}(1-\frac{D}{2})\cdot\int_{r_i}^{r_o}B(\theta)\frac{\pi}{2p}rdr-\int_{r_i}^{r_o}B(\theta)\frac{\pi}{p}rdr\\+\int_{r_i}^{r_o}B(\theta)\frac{\pi}{p}rdr-\int_{r_i}^{r_o}B(\theta)\frac{\pi}{p}rdr+\int_{r_i}^{r_o}B(\theta)\frac{\pi}{2p}rdr\end{matrix}\right\} \quad (23)$$

The magnetic flux is positive when the vector of magnetic flux density has the same direction with the perpendicular vector of the surface element and negative when their directions are opposite. By calculating the above definite integral summation and considering $\theta=\omega_r t$ due to the rotor rotation, the fundamental harmonic component of the magnetic flux as a function of time on the additional winding is obtained, as follows:

$$\Phi(t)=-D\cdot\frac{\pi}{8p}(r_o^2-r_i^2)B_g\sin(\omega_s t) \quad (24)$$

When the demagnetized magnet passes region of the sensor, an oscillation is induced with an amplitude, which is proportional to the demagnetization severity. By employing (7) all over again, for the specific additional winding with N_{sw} turns, and applying (13), the induced voltage is estimated as follows:

$$v_{sw}(t) = N_{sw} D \cdot \frac{\pi}{8} (r_o - r_i)^2 B_g \omega_r \cos(\omega_s t) \qquad (25)$$

It is worth mentioning that under fault condition, the currents in the 3 coils that the supplemental winding spans, are no longer symmetrical, so the resultant magnetic flux that penetrates is non-zero. Since the generator does not have a stator core, it is anticipated that this parasitic effect will not have a strong influence as these generators have a negligible armature reaction field [26].

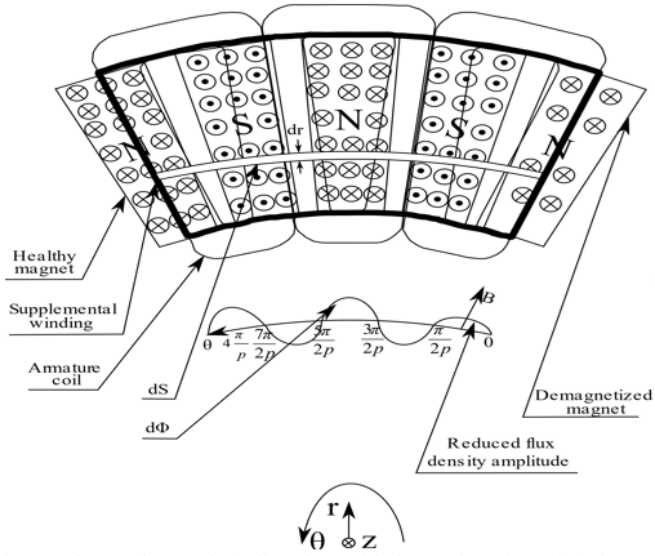

Fig. 3. The supplemental winding along with the 4 pole and 3 coil pitches and the magnet flux density wave that corresponds to that rotor angular position

E. Proposed monitoring signal for partial demagnetization detection

In this subsection, we propose a signal for monitoring the detection of partial demagnetization in AFPM generators. The amplitude of the EMF in a PM generator with a coreless stator is linearly proportional to the rotational speed. Therefore, we propose a fault detection signal in which its shape is used as a fault indicator and its peak-to-peak value is used as fault severity estimator, as follows:

$$FDS(t) = \frac{v_{sw}(t)}{\omega_r(t)} \qquad (26)$$

Under stationary speed conditions, the rotational speed is steady, so it is constant in the above equation. When the rotor of the generator has a varying speed carrying one PM demagnetized in one of its rotors, the signal will remain at the same amplitude due to the speed normalization. Moreover, the fault under nonstationary speed conditions may be diagnosed using the amplitude sideband components of the same signal, which are given by (15) normalized by the rotational speed ω_r, using the frequency components with the pattern of (16).

F. Identification of the partial demagnetization from static and dynamic axis and angular eccentricity conditions

This section demonstrates the analytical derivation of the expected signals, which will be induced on the supplemental winding (sensor) if an eccentricity fault takes place. The term angular eccentricity means the angular rotation of at least one rotor disc around an axis other than the rotational one [21]. A thorough analysis of the defition of both angular and axis eccentricity has been done in [28], [29]. Great care should be given since the term misalignment usually refers to alignment quality between motor and load in radial-flux machines, and not the stator and rotor position. Thus we have avoided to use the term misalignment to describe the two types of eccentricity faults that take place in axial-flux machines. The angular dynamic eccentricity of a rotor is a condition, where the minimum of the air-gap rotates with the mechanical speed, while the airgap is unequal around the circumference. Axial eccentricity has the same concept but the direction of eccentricity but the parallel displacement of rotor in relation to the stator now moves with the mechanical speed. As a result, the voltage on the supplemental winding will consist of continuous oscillations during the whole mechanical period. On the other hand, under a static eccentricity fault the air-gap becomes non-uniform. A voltage will be induced in the sensor coil, which depends on the relative position between sensor and eccentricity, but the signal will be without oscillations.

The analytical formulae for the fault detection signal can be developed by substituting the respective air-gap function for each case in the the permeance function. Eventually, the voltage induced in the supplemental winding under dynamic eccentricity is:

$$E_{DE}(t) = \frac{1}{4} N_c DEF \beta \left(r_o^2 - r_i^2\right) \omega_r \sum_{\nu=2\mu+1}^{\infty} F_{PM,\nu}^{DE} \begin{Bmatrix} \cos\left((\nu p - 1)\frac{4\pi}{p} - \left(\nu - \frac{1}{p}\right)\omega_s t\right) \\ -\cos\left(\left(\nu - \frac{1}{p}\right)\omega_s t\right) \\ +\cos\left((\nu p + 1)\frac{4\pi}{p} - \left(\nu + \frac{1}{p}\right)\omega_s t\right) \\ -\cos\left(\left(\nu + \frac{1}{p}\right)\omega_s t\right) \end{Bmatrix} \qquad (27)$$

and for static eccentricity the voltage in the supplemental winding is:

$$E_{SE}(t) = \frac{1}{4} N_c SEF \beta \left(r_o^2 - r_i^2\right) \omega_r \sum_{\nu=2\mu+1}^{\infty} F_{PM,\nu}^{SE} \begin{Bmatrix} \frac{\nu}{\nu + \frac{1}{p}} \cos\left((\nu p + 1)\frac{4\pi}{p} - \nu\omega_s t\right) + \\ \frac{\nu}{\nu - \frac{1}{p}} \cos\left((\nu p - 1)\frac{4\pi}{p} - \nu\omega_s t\right) + \\ \frac{2p\nu^2}{p\nu^2 - \frac{1}{p}} \cos(\nu\omega_s t) \end{Bmatrix} \qquad (28)$$

From the two above equations the following conclusions may be made. The various faults induce unique voltages in the supplemental winding so this method can be used to distinguish the faults. Moreover, (15) and (27) show that specific harmonic components will be induced in the flux sensor and which are multiple of the inverse pole pair number. However, the partial demagnetization is an abnormality which is not continuous but happens only in the vicinity while the faulty magnet crosses the sensor. The aforementioned show that partial demagnetization and dynamic eccentricity faults can be detected by monitoring the peak-to-peak value of the speed-normalized voltage of the

sensor while it is impossible to mistake static eccentricity for either partial demagnetization or dynamic eccentricity.

III. Finite-Element Analysis and Experimental Validation of the Model

A. Analysis of the partial demagnetization fault and experimental validation of the healthy model

The AFPM generator and the supplemental winding within its air-gap is modelled using a 3-D FEA commercial software package. Fig. 4(a) illustrates the experimental rig of the AFPM generator and Fig. 4(b) graphs the phase voltage. The blue line is the data extracted by the FEA model, and the red line is the phase voltage of the actual generator. This procedure was used to validate the model against the real machine. Fig. 5 shows the model of the three-phase AFPM generator in an exploded view to demonstrate the supplemental winding, which is wound along 3 stator coils. This coil sensor is designed according to the PM geometry with the purpose of obtaining optimized results. The winding of the generator is non-overlapping with coil sequence A-B-C. The major specifications, along with the ones that will be required for analytical calculation of the partial demagnetization factor, are archived in Table I.

Fig. 6 displays two instants in time with 60% partial demagnetization of the axial component of the magnetic flux density value, where the fault detection signal receives its maximum value. The influence of parallel paths creates different values for each magnet due to the different current, which flows in every armature coil for the specific winding configuration. In Fig. 7(a) the no-load axial magnetic field component along a pitch in the middle of the air-gap is plotted for 0-100% demagnetization in incremental steps of 10%. The purpose was to validate that the reduction on the magnetic flux density is linear as there are two magnets in each pitch and that the additional components derived in (15) do not affect the degree of reduction.

The BH characteristic remained linear in the second quadrant for all demagnetization states. In Fig. 7(b) the on-load axial magnetic flux density component along a circle for 50% partial demagnetization is demonstrated for two rotor positions, which corresponds to positions where the fault detection signal takes its maximum value. The purpose is to investigate the magnetic field magnitude distortion due to the armature reaction which the circulating currents create. It appears that the parallel path connections create currents that distort the magnetic flux density wave and cause its value to fluctuate according to the specific winding configuration. As a result, a mean value for the magnetic field magnitudes should be employed for the analytical calculation. The demagnetization fault was emulated by reducing the slope of the BH characteristic in the second quadrant.

TABLE I
Major Specifications of the AFPM Generator

Parameter	VALUE
Apparent Power [kVA]	12.52
No-load voltage line-to-line RMS [kV]	3.86
Rotational speed [r/min]	375
Pole pairs/ Coils	16/24
Turn number of an armature/supplemental coil	640/1
Winding connection	Y
Number of Parallel Paths	4
Magnet-coil clearance [mm]	3.5
Magnet remanence [T]	1.247
Inner/Outer magnet radius [mm]	300/460

In Fig. 8a the fault detection signal during the interval where a magnet crosses the sensor, is plotted for 10 different demagnetization severities in increments of 10%. The peak to peak value increases with the increase in the fault severity level, followed by a lower peak to peak amplitude increments. This means that a selection of peak-to-peak magnitude values can be used as a fault index since the magnet with the specific supplemental coil pitch creates multiple oscillations. Fig. 8b presents the fault detection signal for 50% and 100% demagnetization when the generator has no parallel paths. From the aforementioned it can be concluded that the parallel paths cause additional oscillations in the sensor signal.

(a)

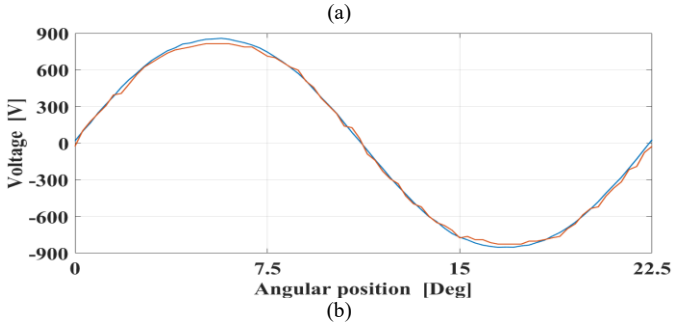

(b)

Fig. 4. (a) Experimental test rig of the AFPM generator to validate the FE model, (b) phase voltage waveform at 100 [r/min] of FE (blue) model and the experimental one (red).

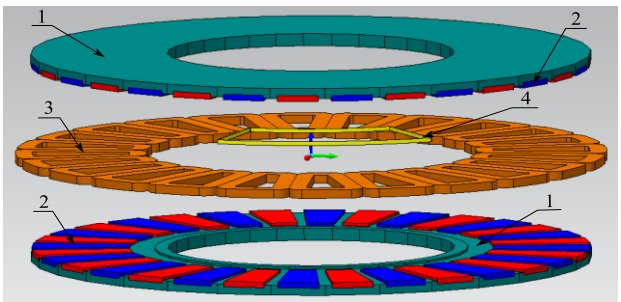

Fig. 5. Exploded view of the AFPMGs' FE model with the additional winding (1) Rotor disc, (2) PM, (3) armature coil of winding, and (4) the supplemental winding.

Fig. 9 illustrates the fault detection signal in time and frequency domain for healthy and two demagnetization cases for a mechanical period. The dB normalization settled with base

1 [mVsec/rad] and not with the fundamental harmonic as it is negated due to the supplemental winding topology.

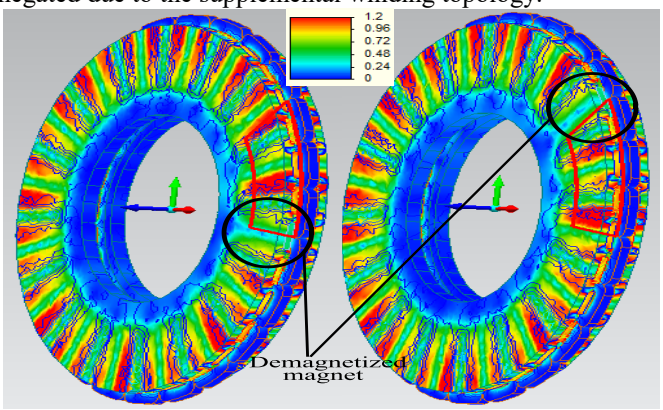

Fig. 6. Field view for rotor position where the voltage on the fault detection signal receives its maximum and minimum value.

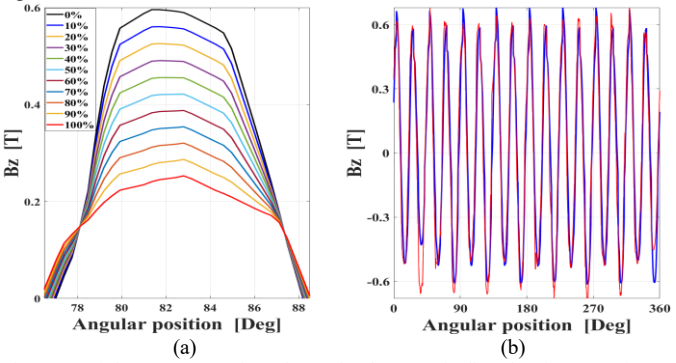

(a) (b)

Fig. 7. Axial component of (a) the no-load magnetic flux density wave for 10 demagnetization severities with 10% step reductions and (b) on-load magnetic flux density when a magnet is demagnetized.

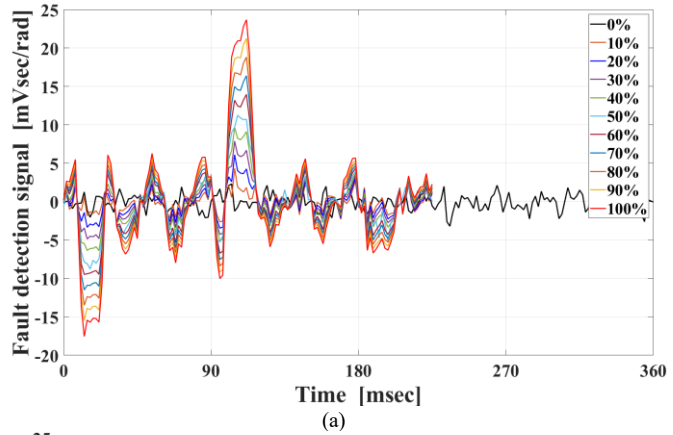

(a)

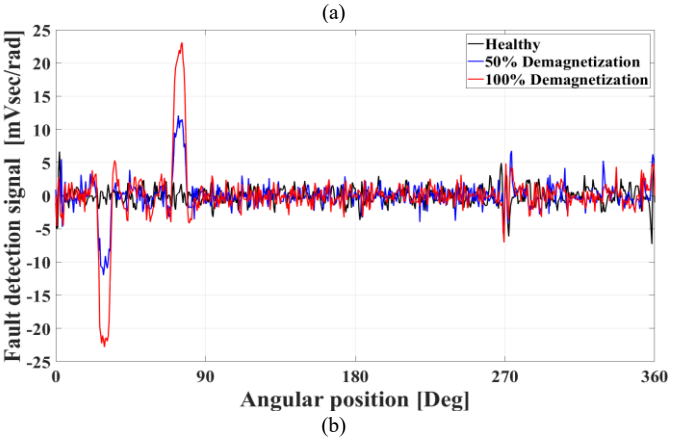

(b)

Fig. 8. Fault detection signal (a) for various demagnetization severity levels of a PM with 4 parallel paths and (b) with no parallel paths for healthy, 50% and 100% demagnetization of a PM.

Under healthy conditions, the signal is approximately zero as shown in Fig. 9a (left graph). There is a small fluctuation caused by the armature reaction end-winding leakage field. Regarding the cases in which a PM was demagnetized for about 40 (Fig. 9b) and 80% (Fig. 9c), oscillations are generated, which depend on only the demagnetization level. This happens because the voltage signal is normalized with speed, and under healthy conditions, the signal approaches zero. With the rise in demagnetization severity, the magnitude of the peak-to-peak magnitude of the oscillation increases linearly. Lastly, the amplitude sidebands with the pattern given by (16) are increased with the demagnetization severity, and their alteration is nonlinear and was theoretically proven by (15).

In Fig. 10 the alteration of the normalized peak-to-peak summation magnitudes for each demagnetization factor is presented. The peak-to-peak value of the fault detection signal can be used as a fault index for partial demagnetization detection. The design parameters can be obtained by consulting Table I, and the air-gap magnetic flux density can be obtained by means of (21), equal to 0.582 [T].To estimate the fault severities for the cases of Fig. 8b which the machine is under and 50% and 100% partial demagnetization we substitude the peak-to-peak amplitude of the fault detection signal in (25) and we obtain 45% and 86% estimation. As a result, the extraction of the peak-to-peak value of the sensor output signal over time and the consideration of the basic machine parameters, can lead to the estimation of the fault severity level.

As shown earlier, due to the parallel-path winding configuration, a further deviation is caused by the analytical model due to the additional oscillations, which slightly reduce the peak-to-peak value of the fault detection signal. However, the peak-to-peak value can still give a decent approximation for the fault severity level.

In Fig. 11a, 11b and 11c the fault detection signal is displayed for healthy 40% and 80% partial demagnetization in time (left) and time-frequency domain (right) under an acceleration of 100 [rpm] in 0.9 seconds starting at a speed of 250 [rpm]. Fig. 11(a) and 11(b) (left columns) validate that the peak-to-peak amplitudes of the fault detection signal remain steady under this state. Moreover, the right columns in Fig. 11 show that the frequency trajectories of the fault harmonics remain steady as the speed increases, and their magnitudes increase only with the fault severity.

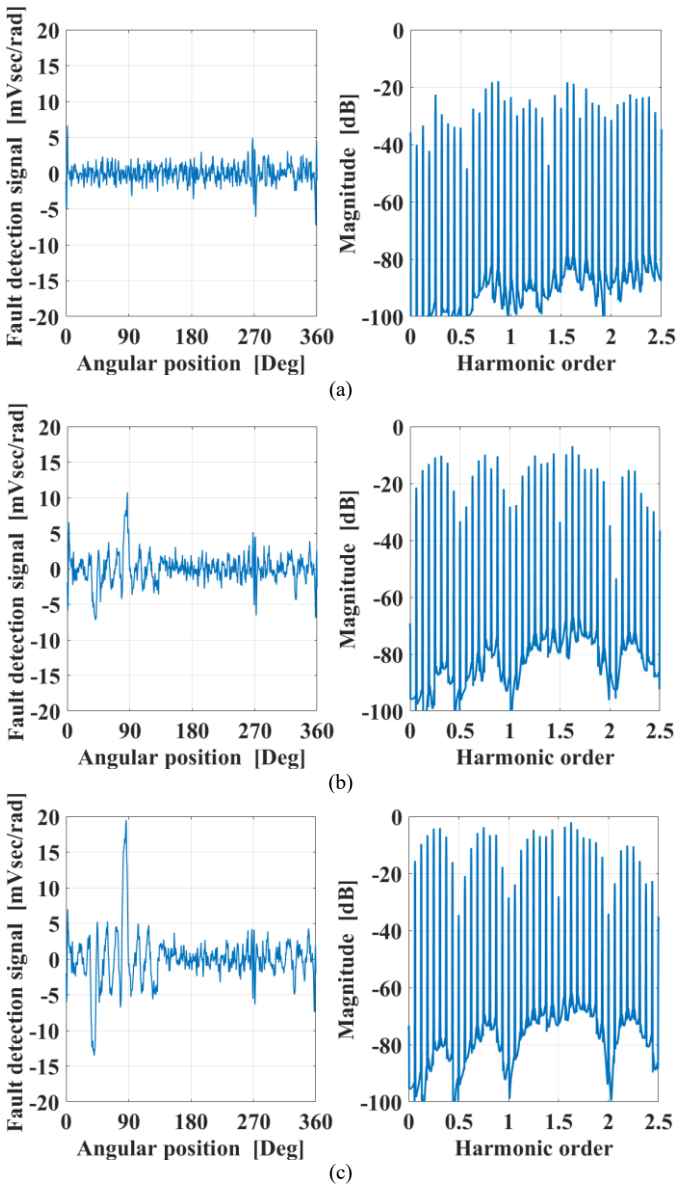

Fig. 9. Fault detection signal in time (left column) and frequency (right column) domain under (a) healthy (b) 40% and (c) 80% partial demagnetization conditions.

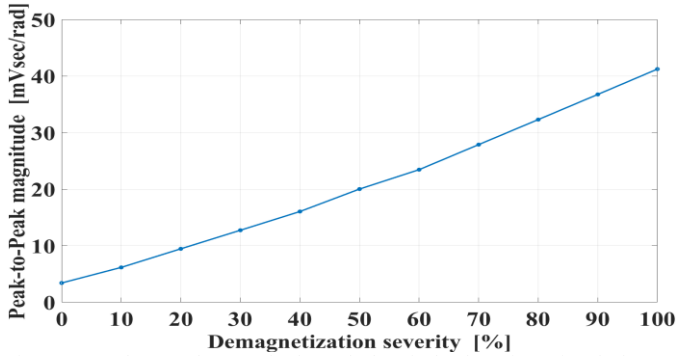

Fig. 10. Peak-to-peak magnitudes of the fault detection signal for 10 demagnetization severities with increments of 10%.

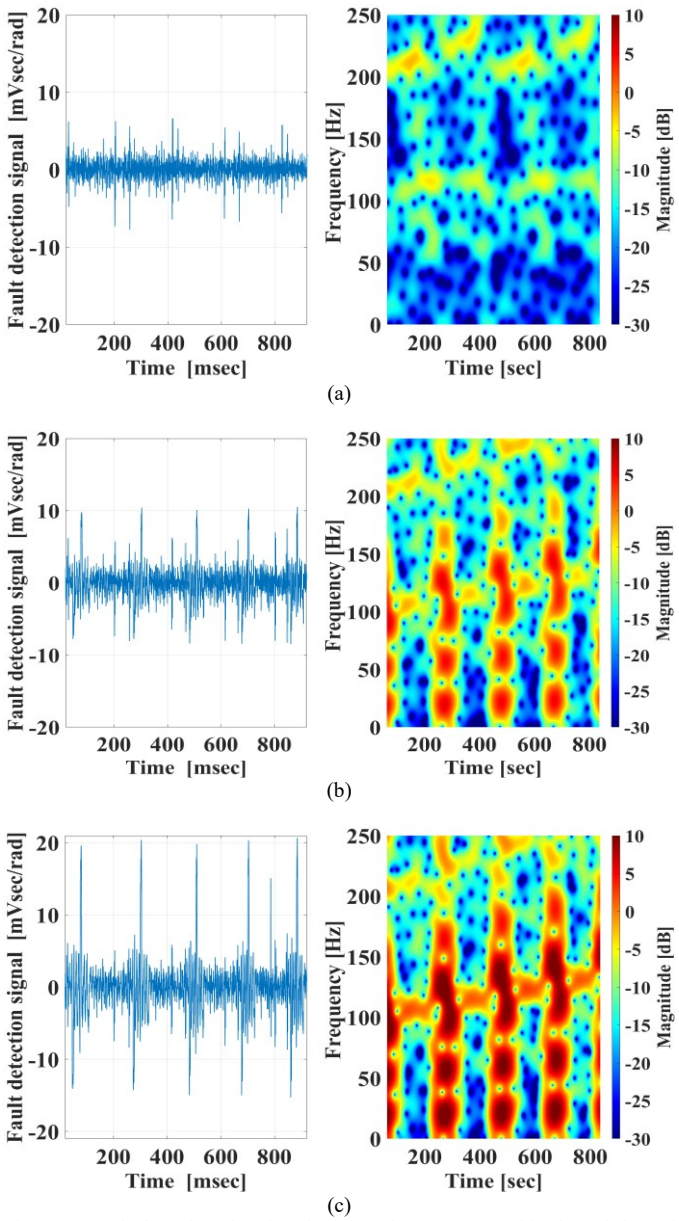

Fig. 11. Fault detection signal under a transient rotor speed in time (left) and time- frequency domain under (a) healthy (b) 40% and (c) 80% partial demagnetization conditions.

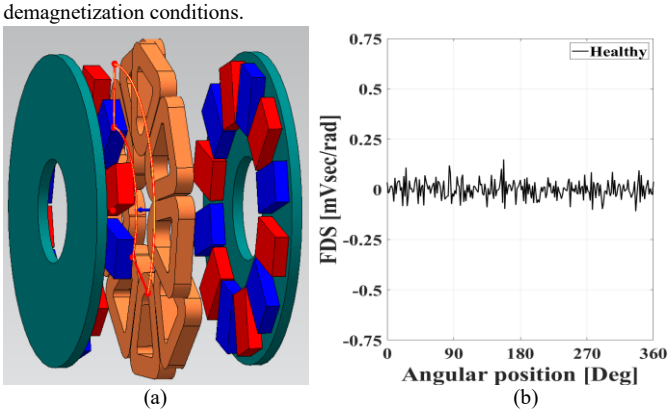

Fig. 12. (a) Model of the axial-flux generator with the search-coil and (b) fault detection signal under healthy condition when the generator rotates at 1000[rpm].

B. Impact of the other faults on the proposed signal

In this subsection, the axis and angular eccentricity faults are extracted using 3-D FEA in an axial-flux generator with purpose to achieve a discrimination with the partial demagnetization fault. In Fig. 12a. the model of the generator is presented with the air-gap search-coil and the fault detection signal for healthy condition, to validate that is zero. The generator has 9 coils and 12 poles and has the same type of winding with the initial. In Fig. 13 the fault detection signal is presented in time domain for the cases of a 70% demagnetized model (which is an equivalent of 35%),unbalanced electric load in which the current in one phase is four times higher, 20% static angular eccentricity, 40% dynamic angular eccentricity, 1 [mm] static axis eccentricity and 2 mm dynamic axis eccentricity. From the figure it can be concluded that for each fault the waveform of the signal is unique. As a result, all faults can be distinguished with each other except the unbalanced electric load fault, since it does have an impact on the search-coil. Moreover, the dynamic faults can be detected since the magnetic flux stays unbalanced on the search-coil along the whole mechanical period. The peak-to-peak magnitude can be used as a fault index. Lastly, the two dynamic faults induce a quite similar waveform on the search-coil. Nevertheless, the waveforms are still distinguishable by inspection.

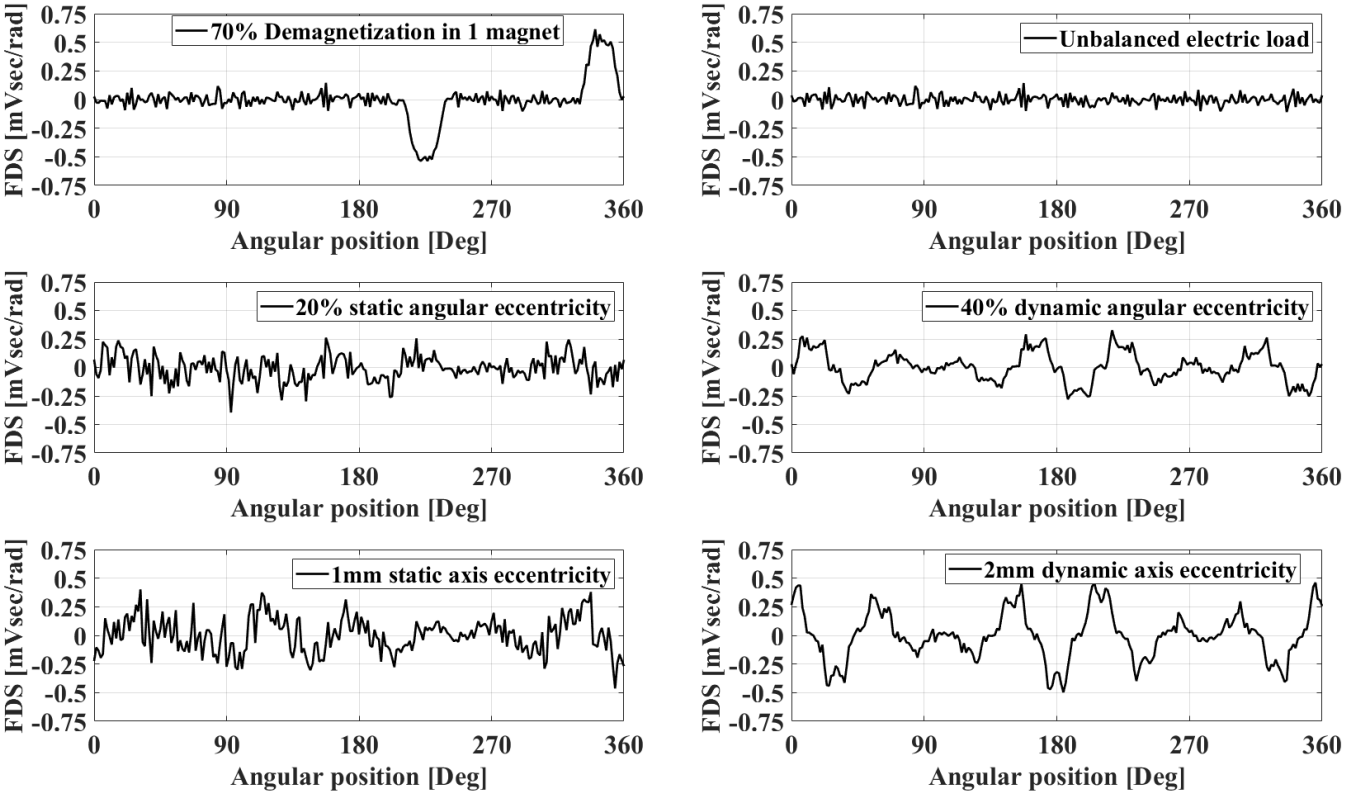

Fig. 13 The speed-normalized voltage signal for all fault cases.

IV. CONCLUSION

This paper proposes a new method for permanent-magnet health monitoring of air-cored axial-flux generators designed for marine energy applications. The peak-to-peak value of the induced speed-normalized voltage on the supplemental winding can be used as a fault indicator signal as it depends only on the fault severity. Signal processing can also be utilized in order to detect the fault using the amplitude-frequency components under steady and variable speed states.

The advantage of this method compared, to a single pitch search-coil, is that the fault can be detected without any further signal processing since the signal is zero under healthy conditions. Moreover, it can detect really low severities since the ripple of the signal is negligible. When the partial demagnetization fault occurs an oscillation is induced on the search-coil in which the peak-to-peak value is connected with the demagnetization severity percentage, according to equation (25).Under uniform demagnetization, the total magnetic flux penetrating the coil is zero, so this technique is only capable of detecting a partial demagnetization fault. The single pitch is able to detect uniform demagnetization since it senses the voltage in each pole pitch.

The dynamic axis and angular eccentricity faults can also be detected, as the fault detection signal will have a different waveform, and the peak-to-peak value can be used as a fault indication in this case too. This method can be utilized in machines in which an additional coil can be implemented, where its span will be capable of negating the voltage under load conditions. The method is applied ideally when there is an even number of pole pitches within the span. If the number of pole pitches is not even, the signal under healthy conditions will not be zero, and the method requires calibration when first implemented. The method which has been demonstrated in the paper can easily be applied to both axial and radial flux PM machines after careful determination of the sensor span, such

that the induced voltage due to the rotor and stator magnetic fields is negated.

APPENDIX

Constants embedded on the equations of Section II

$$\alpha = \frac{\mu_0}{2h_{PM}}\left(1-\frac{g}{h_{PM}}-\frac{t_w}{2h_{PM}}+\frac{g^2}{h_{PM}^2}+\frac{gt_w}{h_{PM}^2}+\frac{t_w^2}{4h_{PM}^2}\right)$$

$$\beta(D) = \frac{\mu_0 D}{2h_{PM}}\left(\frac{g}{2h_{PM}^2\,p}+\frac{t_w}{4h_{PM}\,p}-\frac{1}{2h_{PM}\,p}\right)$$

$$\gamma(D) = \frac{\mu_0}{2h_{PM}}\left\{\left(\frac{D}{2h_{PM}\,p}+\frac{2g}{h_{PM}}+\frac{t_w}{h_{PM}}-1\right)\sum_{k=1}^{\infty}\frac{D}{k\pi h_{PM}}\sin\left(\frac{k\pi}{2p}\right)\right\}$$

REFERENCES

[1] K. Sitapati and R. Krishnan, "Performance comparisons of radial and axial field, permanent-magnet, brushless machines," *IEEE Trans. Ind. Appl.*, vol. 37, no. 5, pp. 1219–1226, 2001.

[2] J. Hong *et al.*, "Detection and classification of rotor demagnetization and eccentricity faults for PM synchronous motors," *IEEE Trans. Ind. Appl.*, vol. 48, no. 3, pp. 923–932, 2012.

[3] J. Hong, D. Hyun, S. Bin Lee, J. Y. Yoo, and K. W. Lee, "Automated monitoring of magnet quality for permanent-magnet synchronous motors at standstill," *IEEE Trans. Ind. Appl.*, vol. 46, no. 4, pp. 1397–1405, 2010.

[4] A. A. El-Moneim, A. Gebert, F. Schneider, O. Gutfleisch, and L. Schultz, "Grain growth effects on the corrosion behavior of nanocrystalline NdFeB magnets," *Corros. Sci.*, vol. 44, no. 5, pp. 1097–1112, 2002.

[5] J. R. Riba Ruiz, J. A. Rosero, A. Garcia Espinosa, and L. Romeral, "Detection of demagnetization faults in permanent-Magnet synchronous motors under nonstationary conditions," *IEEE Trans. Magn.*, vol. 45, no. 7, pp. 2961–2969, 2009.

[6] K. Kim, S. Lim, and J. Lee, "The design of permanent magnet synchronous motor considering partial demagnetization on the permanent magnet," *INTERMAG 2006 - IEEE Int. Magn. Conf.*, vol. 42, no. 10, p. 309, 2006.

[7] J. Faiz and E. Mazaheri-Tehrani, "Demagnetization Modeling and Fault Diagnosing Techniques in Permanent Magnet Machines under Stationary and Nonstationary Conditions: An Overview," *IEEE Trans. Ind. Appl.*, vol. 53, no. 3, pp. 2772–2785, 2017.

[8] D. Torregrossa, A. Khoobroo, and B. Fahimi, "Prediction of acoustic noise and torque pulsation in PM synchronous machines with static eccentricity and partial demagnetization using field reconstruction method," *IEEE Trans. Ind. Electron.*, vol. 59, no. 2, pp. 934–944, 2012.

[9] J. C. Urresty, R. Atashkhooei, J. R. Riba, L. Romeral, and S. Royo, "Shaft trajectory analysis in a partially demagnetized permanent-magnet synchronous motor," *IEEE Trans. Ind. Electron.*, vol. 60, no. 8, pp. 3454–3461, 2013.

[10] J. Hong, S. Bin Lee, C. Kral, and A. Haumer, "Detection of airgap eccentricity for permanent magnet synchronous motors based on the d-axis inductance," *IEEE Trans. Power Electron.*, vol. 27, no. 5, pp. 2605–2612, 2012.

[11] R. Z. Haddad and E. G. Strangas, "On the Accuracy of Fault Detection and Separation in Permanent Magnet Synchronous Machines Using MCSA/MVSA and LDA," *IEEE Trans. Energy Convers.*, vol. 31, no. 3, pp. 924–934, 2016.

[12] A. Mohammed, J. I. Melecio, and S. Durovic, "Electrical Machine Permanent Magnets Health Monitoring and Diagnosis Using an Air-Gap Magnetic Sensor," *IEEE Sens. J.*, vol. 20, no. 10, pp. 5251–5259, 2020.

[13] T. Goktas, M. Zafarani, and B. Akin, "Discernment of Broken Magnet and Static Eccentricity Faults in Permanent Magnet Synchronous Motors," *IEEE Trans. Energy Convers.*, vol. 31, no. 2, pp. 578–587, 2016.

[14] M. Zafarani, T. Goktas, and B. Akin, "A comprehensive magnet defect fault analysis of permanent magnet synchronous motors," *IEEE Trans. Ind. Appl.*, vol. 2015, no. 2, pp. 1331–1339, 2015.

[15] C. Ruschetti, C. Verucchi, G. Bossio, C. De Angelo, and G. García, "Rotor demagnetization effects on permanent magnet synchronous machines," *Energy Convers. Manag.*, vol. 74, pp. 1–8, 2013.

[16] E. Maruyama, A. Nakahara, A. Takahashi, and K. Miyata, "Circulating current in parallel connected stator windings due to rotor eccentricity in permanent magnet motors," *2013 IEEE Energy Convers. Congr. Expo. ECCE 2013*, pp. 2850–2855, 2013.

[17] I. P. Brown, D. M. Ionel, and D. G. Dorrell, "Influence of parallel paths on current-regulated sine-wave interior-permanent-magnet machines with rotor eccentricity," *IEEE Trans. Ind. Appl.*, vol. 48, no. 2, pp. 642–652, 2012.

[18] Y. Park *et al.*, "Online detection and classification of rotor and load defects in PMSMs Based on Hall sensor measurements," *IEEE Trans. Ind. Appl.*, vol. 55, no. 4, pp. 3803–3812, 2019.

[19] D. Reigosa, D. Fernandez, M. Martinez, Y. Park, S. Bin Lee, and F. Briz, "Permanent Magnet Synchronous Machine Non-Uniform Demagnetization Detection Using Zero-Sequence Magnetic Field Density," *IEEE Trans. Ind. Appl.*, vol. 55, no. 4, pp. 3823–3833, 2019.

[20] D. Reigosa, D. Fernandez, Y. Park, A. B. Diez, S. Bin Lee, and F. Briz, "Detection of Demagnetization in Permanent Magnet Synchronous Machines Using Hall-Effect Sensors," *IEEE Trans. Ind. Appl.*, vol. 54, no. 4, pp. 3338–3349, 2018.

[21] S. M. Mirimani, A. Vahedi, F. Marignetti, and R. Di Stefano, "An online method for static eccentricity fault detection in axial flux machines," *IEEE Trans. Ind. Electron.*, vol. 62, no. 3, pp. 1931–1942, 2015.

[22] K. Kang, J. Song, C. Kang, S. Sung, and G. Jang, "Real-Time Detection of the Dynamic Eccentricity in Permanent-Magnet Synchronous Motors by Monitoring Speed and Back EMF Induced in an Additional Winding," *IEEE Trans. Ind. Electron.*, vol. 64, no. 9, pp. 7191–7200, 2017.

[23] Y. Da, X. Shi, and M. Krishnamurthy, "A new approach to fault diagnostics for permanent magnet synchronous machines using electromagnetic signature analysis," *IEEE Trans. Power Electron.*, vol. 28, no. 8, pp. 4104–4112, 2013.

[24] E. G. Strangas, S. Aviyente, and S. S. H. Zaidi, "Time-frequency analysis for efficient fault diagnosis and failure prognosis for interior permanent-magnet AC motors," *IEEE Trans. Ind. Electron.*, vol. 55, no. 12, pp. 4191–4199, 2008.

[25] J. C. Urresty, J. R. Riba, and L. Romeral, "Influence of the stator windings configuration in the currents and zero-sequence voltage harmonics in permanent magnet synchronous motors with demagnetization faults," *IEEE Trans. Magn.*, vol. 49, no. 8, pp. 4885–4893, 2013.

[26] J. F. Gieras, R. J. Wang, and M. J. Kamper, *Axial flux permanent magnet brushless machines*. 2005.

[27] M. J. Kamper, R. J. Wang, and F. G. Rossouw, "Analysis and performance of axial flux permanent-magnet machine with air-cored nonoverlapping concentrated stator windings," *IEEE Trans. Ind. Appl.*, vol. 44, no. 5, pp. 1495–1504, 2008.

[28] M. Thiele and G. Heins, "Computationally Efficient Method for Identifying Manufacturing Induced Rotor and Stator Misalignment in Permanent Magnet Brushless Machines," *IEEE Trans. Ind. Appl.*, vol. 52, no. 4, pp. 3033–3040, 2016.

[29] B. Guo, Y. Huang, F. Peng, J. Dong, and Y. Li, "Analytical Modeling of Misalignment in Axial Flux Machine," *IEEE Trans. Ind. Electron.*,vol. 67, no. 6, pp. 4433–4443, 2020.